Md Ashraful Haque[a], Tony G. Feric[b,d], Sara T. Hamilton[c,d], Ah-Hyung Alissa Park[b,c,d],

Mark D. Dadmun[a,*]

[a]Department of Chemistry

The University of Tennessee, Knoxville, TN, 37996, USA

[b]Department of Chemical Engineering,

Columbia University, New York, NY 10027, USA

[c]Department of Earth and Environmental Engineering,

Columbia University, New York, NY 10027, USA

[d]Lenfest Center for Sustainable Energy, The Earth Institute,

Columbia University, New York, NY 10027, USA

* Corresponding author, Dad@utk.edu

Abstract

Recently, nanoparticle organic hybrid materials (NOHMs) have been considered as promising electrolytes for energy storage applications due to their unique combination of properties, which include high thermal stability, negligible vapor pressure and easy synthesis. However, the structural features of NOHMs in electrochemical systems is not well understood. Hence, we investigate the impact of grafting type (ionic vs covalent) on the structure and performance of NOHMs that consist of a silica core and grafted HPE polymer (Jeffamine M2070) in aqueous solution with and without the presence of supporting electrolyte (0.1 M $KHCO_3$) using small-angle neutron scattering. Careful analyses of the results indicates that even at low grafting density (0.8 chains nm^{-2}) and concentration (1-3 wt.%), ionic NOHMs solutions contain free polymer that may interact with the grafted polymer, altering the assembly of NOHMs in solution. Our investigation also elucidates that the covalent NOHMs solutions consist of both aggregated and dispersed NOHMs in the solution. Moreover, the addition of supporting electrolyte affects the assembly and structure of polymer in the ionic NOHMs solution significantly, whereas only a slight change in conformation of the grafted polymer is observed for covalent NOHMs. These conformational changes alter the performance of NOHMs solution, resulting in a dramatic change in viscosity. Careful analysis shows that this significant alteration of solution viscosity in the ionic NOHMs can be traced back to the presence of the free polymer that interacts with the grafted layer, and the attenuation of this interaction between free and grafted polymer with the addition of salt. Thus, these studies elucidate the impact of grafting type on the overall structure, assembly, and performance of functionalized NOHMs in aqueous solution, and explicitly correlates the structure and assembly of NOHMs to their transport properties and must be considered when designing functional systems that incorporate NOHMs.

Keywords

Nanoparticle Organic Hybrid Materials, Grafted polymer, Structure, Nanoparticle Assembly, Small-angle neutron scattering

Introduction

The need to reduce carbon emissions and fossil fuel usage to prepare for a sustainable future has motivated current researchers to search for environment-friendly materials and processes for energy production and storage. The use of renewable energy can relieve some of the demand of fossil fuels and consequently can reduce our carbon footprint.[1,2] However, the intermittency of renewable energy has challenged the successful utilization of this source in the existing power-grid.[3,4] Hence, energy storage systems, such as redox flow batteries (RFB), are needed to harness the production of renewable energy sources.[5,6] There are several limitations of redox flow batteries including conductivity, solubility of redox species and a narrow electrochemical window that require attention to realize their potential.[7–9] The rational design of novel electrolytes can play a key role in overcoming these limitations of RFBs. For instance, ionic liquids (ILs),[6,10–12] microemulsions,[13–16] and deep eutectic solvents (DESs)[17–19] have recently gained attention as candidates to deploy as novel electrolytes in energy storage systems for their attractive properties. Nanoparticle organic hybrid materials (NOHMs) are also an interesting candidate as novel electrolytes that have gained attention for their unique properties including negligible vapor pressure,[20] high oxidative-thermal stability[21–25] and tunable chemistry.[26,27]

Nanoparticle organic hybrid materials (NOHMs) consist of an inorganic core with an organic polymer canopy grafted to the core ionically or covalently. This class of polymer grafted nanoparticles has been extensively studied and these materials have been shown to improve the performance of lithium batteries[28–30] and to efficiently capture CO_2 with high loading capacities.[20,24,31–35] Moreover, the opportunity to alter the ligand chemistry,[35] the corona connectivity[26,36] and the nanoparticles[37] offers tunability in the performance of NOHMs, making them an attractive choice for energy storage systems, as well as integrated CO_2 capture and

conversion applications.[35,38] However, NOHMs suffer from high viscosity that can limit their performance and often requires them to be used as additives in solution in an electrochemical system.[20,39,40] Solubilizing NOHMs in an aqueous solution reduces the viscosity significantly,[20] potentially overcoming an apparent barrier of the use of NOHMs as an electrolyte component. However, solubilizing the NOHMs can alter the structure and assembly of the NOHMs, and correlating these structural characteristics to performance is needed to effectively implement them in energy storage systems. This is essential as the transport and structural properties of electrolytes have been shown to dictate the overall electrochemical performance.[41–45]

Recently, NOHMs solutions have been extensively investigated to develop an understanding of their structure and transport mechanism in energy storage systems. These studies show that factors such as pH, salt addition, secondary fluid properties (e.g., polarity, hydrogen bonding ability and molar volume) and NOHM concentration can significantly impact the conformation, assembly, and ordering of the ionically tethered polymer canopy in NOHMs.[39,40,46,47] For instance, Cantillo et. al. showed that the complexation of Cu^{2+} with the ionically tethered polyethylenimine (PEI) polymer canopy can be altered by tuning the pH of the system.[46] Moreover, Hamilton et. al. also showed in a different study that the polymer conformation of ionic NOHMs can be altered by adding and removing salt (e.g., ionic stimulus) in the solution.[40] Feric et. al. have highlighted the effect of the secondary fluid properties on the

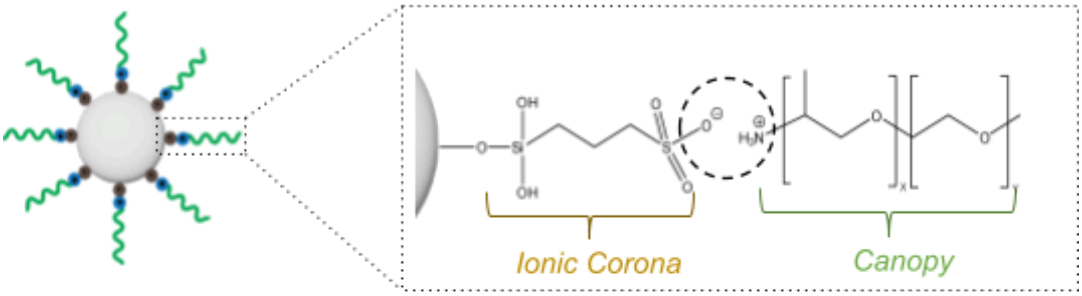

diffusion coefficient and viscosity of the ionically tethered polymer in NOHMs and showed that the interaction of the polymer with the nanoparticle surface can be modified by the different secondary fluids.[39] In our previous study using small-angle neutron scattering (SANS) experiments, we investigated the structure and assembly of a series of ionic NOHMs in aqueous solution with NOHMs loadings of 10 - 40 wt.%.[47] These results showed that the aqueous solutions of NOHMs with a grafting density of 2-2.5 chains nm^{-2} contained a significant amount of free polymer in the solution at these concentrations. The results of this work suggested that free polymers in solution can interact with the grafted polymer and thus, changes the molecular assembly of the polymer near the nanoparticle surface. To expand our understanding of NOHMs in functional applications, we have completed similar experiments on NOHMs with a much lower polymer grafting density and NOHMs that the polymer covalently bound to the nanoparticle, where a tethering-untethering process is precluded. The experiments on covalently bound NOHMs elucidate the importance of the grafting type, and thus the tethering-untethering equilibrium of the grafted polymer, the structure of NOHMs-based fluids, as well as the impact of added electrolyte salt on their structure and dynamics.

Thus, we have investigated the structure and assembly of NOHM-I-$HPE_{0.8}$, NOHM-C-$HPE_{0.5}$, NOHM-C-$HPE_{0.7}$ (grafting densities are included as subscript), which have an inorganic silica core and grafted HPE (Jeffamine M2070) canopy at identical concentrations using small angle neutron scattering (SANS). SANS offers information on the conformation of the free and grafted polymer, as well as the structure of the grafted layer. A graphical representation of the structure of the ionic and covalent NOHMs is given in Figure 1.

Investigating the structure and assembly of the ionic and covalent NOHMs offers insight into the dispersion and conformation of grafted and free polymer in the NOHMs aqueous

solution. Additionally, our results investigate the impact of added salt on the conformation of the free and grafted polymer and how this assembly subsequently impacts the viscosity of the solution. A small portion of the SANS results of this study has been reported.[21] However, in this study, we provide a more complete analysis of the small angle neutron scattering results that include the investigation of the conformation of untethered HPE polymer, the amount of free polymer in ionic NOHMs at lower concentrations, the extent of aggregation in covalent NOHMs and a direct correlation of the structure of untethered HPE polymer and NOHMs assembly to their transport properties which reveals the impact of grafting type on the complex assembly of NOHMs in aqueous solution.

Materials & Method

Synthesis of Ionically bound NOHMs (NOHM-I-HPE):

NOHM-I-HPE was synthesized to a targeted grafting density (0.8 chains nm^{-2}) using a process similar to that reported previously.[20,25,32,34,36,39,48] In short, a 1 wt.% solution of the ionic linker, 3-(trihydroxysilyl)-1-propane-sulfonic acid (Gelest Inc.) was added to a 4 wt.% SiO_2 nanoparticle (LUDOX SM-30 obtained from Sigma-Aldrich) solution in a dropwise manner. The resulting surface coverage of silica nanoparticles is expected to be ≈2.0 chains nm^{-2} after the addition of the ionic linker. Then, the pH of the solution was adjusted to 5 by the addition of 1 M NaOH in the solution and subsequently, the solution was stirred at 70 °C for 24 h. The functionalized silica nanoparticles were then passed through a cation exchange resin (Dowex Marathon C hydrogen form, Sigma Aldrich) to protonate the linker molecules and remove any excess cations. 20 wt.% Jeffamine M2070 polymer (MW = 2000 g mol^{-1}, acquired from Huntsman Co., referred to as HPE) was added dropwise resulting in grafting density of 1.0

chains nm^{-2}, prior to sample purification. After mixing overnight at room temperature, the solution was dialyzed for at least 48 h (SnakeSkin Dialysis Tubing 10K MW cutoff, Thermo Scientific) to remove any untethered polymer, with frequent water changing. To confirm the removal of excess water, the solution was placed in an oven at 60 °C overnight. Thermogravimetric analysis (TGA) revealed that the sample obtained a final grafting density of 0.8 chains nm^{-2}.

Synthesis of Covalently bound NOHMs (NOHM-C-HPE):

A previous protocol was also used to synthesize NOHM-C-HPE at the targeted grafting densities.[20,26,36] In this process, 3 wt.% of HPE dissolved in ethanol is mixed with 3 wt.% of (3-glycidyloxypropyl) trimethoxysilane (acquired from Gelest Inc. and referred to as GPC) in ethanol. To complete the reaction between the HPE chains and the GPC linker, the mixture was then stirred at 50 °C for 12 hours. After the completion of the reaction, a distillation process was used to remove the ethanol resulting in the functionalized HPE polymer. The HPE polymer was then dissolved in deionized water to a concentration of 7 wt.% that was then mixed with 3 wt.% of silica nanoparticles (LUDOX SM-30 obtained from Sigma-Aldrich). Similar to the NOHM-I-HPE synthesis, the mixture of HPE polymer and silica nanoparticles was then left overnight to mix. The mixture then went through a 48 h dialysis process. To remove excess water, the mixture was left in a vacuum oven overnight at 60 °C. Although the target grafting density was 1.0 and 2.0 chains nm^{-2}, TGA analysis revealed that the final sample achieved a grafting density of 0.5 and 0.7 chains nm^{-2}.

Small-Angle Neutron Scattering:

The samples of 1 wt.% and 3 wt.% of NOHM-I-HPE$_{0.8}$, NOHM-C-HPE$_{0.5}$, NOHM-C-HPE$_{0.7}$ and 1 wt.% and 5 wt.% of HPE were prepared by dissolving in D_2O. Samples of NOHM-I-HPE$_{0.8}$, NOHM-C-HPE$_{0.5}$, NOHM-C-HPE$_{0.7}$ and HPE at identical concentrations were also prepared by dissolving in D_2O with added 0.1 M $KHCO_3$ salt. The SANS experiments were performed at a Q range of 0.001–0.8 Å at the HFIR CG-2 GP SANS beamline located at the Oak Ridge National Laboratory. The wave vector, Q, is $= 4\pi/\lambda \sin(\theta)$, where λ is the neutron wavelength and θ is the scattering angle. The coherent scattering profiles were obtained using the Jupyter software program that corrected for the empty cell scattering, thickness of the cell, transmission of the sample, and solvent scattering. The small angle scattering analysis software package SasView was used to fit and analyze the scattering profiles of the HPE, NOHM-I-HPE, and NOHM-C-HPE solutions.[49]

Viscosity:

The viscosity of aqueous solutions of HPE, NOHM-I-HPE, and NOHM-C-HPE with and without the presence of salt (0.1 M $KHCO_3$), were measured using a VISCOlab 4000 (Cambridge Viscosity – PAC) viscometer. This viscometer can measure viscosities from 0.2 to 10000 cP. While measuring the viscosity of the samples, the temperature was controlled at 25.00 ±0.05 °C using a water bath (VWR 1166D). The error in viscosity was within ±5% for all the samples.

Discussion and Results:

Impact of grafting type (Ionic vs Covalent) on the Structure and Assembly of NOHMs in aqueous solution

Conformation of HPE polymer in Solution

The structure and conformation of the untethered HPE polymer in solution without nanoparticles is examined first to provide a basis to understand the impact of the nanoparticle on the structure and assembly of the free polymer. The SANS profiles of 1 wt.% and 5 wt.% HPE in D_2O are shown in Figures S1 and S2, respectively. These figures also show the fits of the data to the polymer excluded volume model, from which the radius of gyration (R_g) and Porod exponent (which correlates to the mass fractal dimension of the polymer chain) can be determined. The mass fractal dimension documents the compactness of the polymer chain over length scales below the radius of gyration (R_g) and above the statistical length (b) of the polymer, and corresponds to a q range of $1/R_g < q < 1/b$.[50] The fractal dimension is often correlated to the Flory exponent where the fractal dimension scales inversely with the Flory exponent. The Flory exponent provides insight on the conformation of the polymer in a solvent, where a Flory exponent, $\nu = 0.5$, refers to a θ (theta) solvent in which a polymer follows a random walk conformation and $\nu = 0.33$ refers to poor solvent and a collapsed polymer chain.[51] Table 1 below shows the radius of gyrations and Flory exponents of the HPE polymer in aqueous solution that emerge from this fitting process. These results indicate that the radius of gyration of the polymer varies from ~17 to ~12 Å. Moreover, the Flory exponent shows that the polymer chain is not expanded in water.

Table 1. Radius of gyration and Flory exponent of HPE polymer in aqueous solution obtained from polymer excluded volume fits of the SANS curves.

Sample	R_g (Å) ± 1 Å	Flory exponent, ν
1 wt.% HPE	17	0.50
1 wt.% HPE 0.1 M $KHCO_3$	15	0.39
5 wt.% HPE	13	0.50
5 wt.% HPE 0.1 M $KHCO_3$	12	0.41

From the Flory exponent values, it is evident that water is a θ (theta) solvent (ν = 0.5) for the HPE polymer, and the polymer follows a random walk model. This result is consistent with the study done by Feric et al. where HPE polymer in aqueous solution showed that the scaling of diffusion with concentration resembles that of an ideal polymer conformation.[39] With the addition of salt, the Flory exponent decreases indicating that the polymer chain collapses, consistent with the decrease in R_g. This conformational analysis of HPE polymer provides a foundation to interpret the scattering analysis of the NOHMs solutions more fully.

Structure of ionic NOHMs in solution

With the goal of understanding the impact of grafting bond type on the structure and assembly of NOHMs in solutions, the neutron scattering profile of NOHM-I-HPE and NOHM-C-HPE with similar grafting density and concentration were measured. In our previous study of the structure of ionically bonded NOHMs in solution (NOHM-I-$HPE_{2\text{-}2.5}$), the scattering profiles of the solutions showed a decrease in intensity at low Q ($Q \lesssim 0.1$ $Å^{-1}$) and an increase in intensity at high-q ($Q \gtrsim 0.1$ $Å^{-1}$) with increasing concentration of NOHMs, which is a result of the presence of free polymer.[47] The NOHM-I-HPE used in this previous work had a grafting density of 2.0-2.5 chain nm^{-2} corresponding to a significant amount of free polymer. However, in order to compare the structure and assembly of similar ionic and covalent NOHMs solutions, it was necessary to decrease the grafting density, and decrease the NOHM concentration due to the limited miscibility of the covalent NOHMs in solution. Thus, the SANS profile of covalent and ionic NOHMs at 1 wt.% and 3 wt.% with grafting densities of 0.5-0.8 chains nm^{-2} were collected.

Figure S3 shows the scattering profile of 1 wt.% and 3 wt.% NOHM-I-HPE with a grafting density of 0.8 chains nm^{-2}. Initially, only the core-shell sphere model with a square well

structure factor was used to fit the scattering profile. However, this model fails to fit the full scattering profile of these samples. However, inclusion of the polymer excluded volume model with the core-shell sphere model captures the whole scattering profile. This is similar to our previous studies and indicates that the solution consists of NOHMs as well as free polymer in solution. The fits of the SANS profiles of 1 wt.% and the 3 wt.% NOHM-I-HPE$_{0.8}$ to this model are provided in Figure S4. In the analysis of the data with this model, the radius (~4.5 nm) and the scattering length density of the silica nanoparticle (~4.4E-06 Å^{-2}) are kept constant. The scattering length density of the grafted layer and the solvent, the thickness of the grafted layer and the radius of gyration of the free polymer are then fitted in the analysis. The results of this successful fitting process provide valuable information on the structure and assembly of the NOHM-I-HPE and free polymer in solution, including the

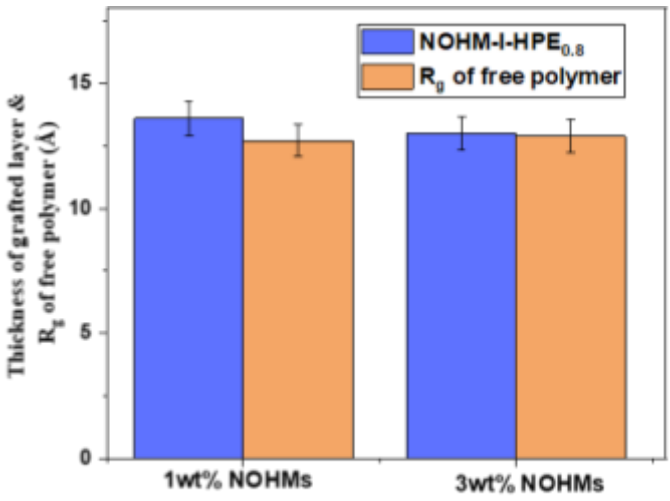

Figure 3. Thickness of grafted layer of NOHM-I-HPE$_{0.8}$ and R$_g$ of free polymer.

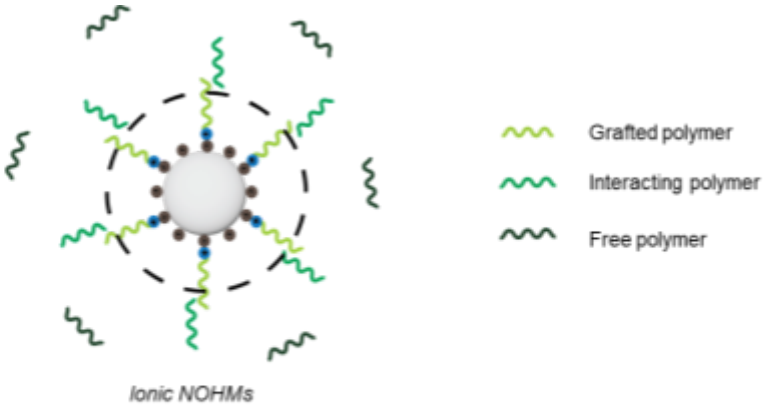

Figure 2. Illustration of the structure and assembly of free polymer, *interacting polymer* and grafted polymer in NOHM-I-HPE solution

conformation of the free polymer and concentration dependence of the thickness of the grafted layer of NOHM-I-HPE$_{0.8}$. Figure 2 shows a graphical representation of the structure and assembly of free polymer and grafted free polymer in these NOHM-I-HPE solutions. Figure 3 plots the thickness of the grafted layer and the radius of the gyration of the free polymer at both 1 wt.% and 3 wt.% loadings. The result shows that the thickness of the grafted layer and the radius of gyration of the free polymer are very similar ~13-14 Å. The R_g of the polymer in solution at 1 wt.% has been measured to be 17 Å, indicating that the presence of the nanoparticle in solution collapses the polymer chain slightly.

The model also provides insight into the amount of free polymer that is present in the NOHM-I-HPE$_{0.8}$ solution. Equation 1 shows the analytical relationship between the concentration of free polymer and the experimentally measured scattering length density (SLD) of the solvent in the NOHMs samples.

$$\Phi_1 = \frac{SLD_{solv} - SLD_{D_2O}}{SLD_{poly} - SLD_{D_2O}} \qquad \mathbf{1}$$

In Equation 1, (Φ_1) is the volume fraction of free polymer in the solvent, SLD_{poly} is the SLD of polymer = 0.517E-06 Å^{-2}, SLD_{D2O} is the SLD of D_2O = 6.35E-06 Å^{-2}, and SLD_{solv} is the experimentally determined SLD of the solvent, which is a mixture of the free polymer and D_2O. Using Equation 1, the volume fraction of free polymer in the solvent is determined to be 0.005 (±.00025). This corresponds to an average of 42 vol.% of the polymer present in the sample being free polymer. This indicates that a significant portion of the free polymer is present in the 1 wt.% and 3 wt.% NOHM-I-HPE$_{0.8}$ aqueous solutions.

Moreover, our previous studies clearly demonstrated that the free polymer penetrates and interacts with the grafted layer at NOHMs loadings above 15 wt.%.[47] However, in these studies,

the similarity of the R_g of the grafted layer and that of the free polymer indicates that at these lower NOHMs concentrations, there is minimal impact of the presence of the free polymer on the conformation of the grafted layer.

Structure of Covalent NOHMs in solution

To provide insight into the impact of the grafting type on the structure and assembly of the NOHMs in aqueous solution, the SANS profiles of the covalently bound NOHMs are similarly analyzed. Figure 4 compares the 1 wt.% and 3 wt.% NOHM-C-HPE scattering profiles to those of the NOHM-I-HPE solutions. Figure 4 shows the scattering intensity of the NOHM-C-HPE solutions are higher than that of NOHM-I-HPE, indicating the presence of aggregates in the NOHM-C-HPE solution. This is verified by the fact that the core-shell model no longer fits the scattering of the covalently bound samples. Thus, a model that accounts for NOHM aggregation is utilized, the fractal core-shell model, which captures the scattering effects from fractal aggregates that are formed from core-shell particles. The fractal core-shell model provides structural information of the fractal aggregates as well as the structure of the core-shell NOHMs in the sample, including the thickness of the grafted layer.

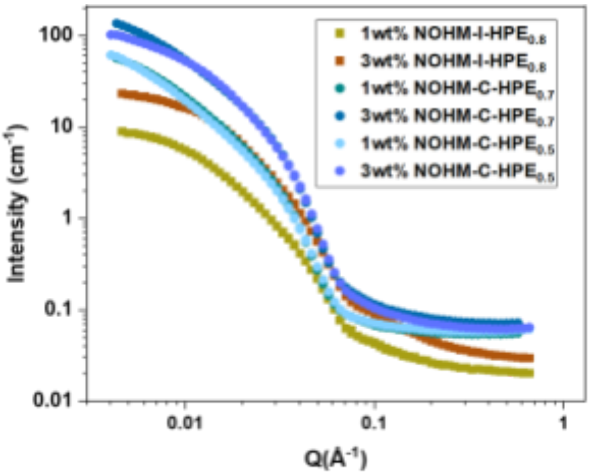

Figure 4. Small-angle neutron scattering profile of 1 wt.% and 3 wt.% NOHM-I-$HPE_{0.8}$, NOHM-C-$HPE_{0.7}$, NOHM-C-$HPE_{0.5}$ in aqueous solution.

In fact, fitting the scattering profile of covalent NOHMs using only the fractal model does not capture the scattering over the entire Q range, especially at high q ($0.08\ Å^{-1} < Q < 0.1\ Å^{-1}$),

which corresponds to length scales of ~62 Å -78 Å. The excess scattering at these length scales is consistent with the presence of *dispersed individual* covalent NOHMs particles in the solution. Therefore, a scattering model that combines fractal core-shell (aggregates) and core-shell spheres (individual NOHMs) is used to capture the total scattering of covalent NOHMs solutions. Figure S5 show SANS profiles and the fits to this model of the 1 wt.% and 3 wt.% NOHM-C-HPE aqueous solution at different grafting densities. The analysis of the scattering curves by this fitting process documents the extent of aggregation of the NOHM-C-HPE in solution. The fitting process also provides mass fractal dimension of the aggregates, which correlates to the compactness of the aggregates. Figure S6 illustrates the correlation between mass fractal dimensions and compactness of the aggregates. The mass fractal dimension can range from 1 to 3 where 1 corresponds to linear aggregates, whereas 3 refers to condensed compact aggregates.[52,53] The fractal dimension of the covalent NOHMs aggregates in solution is ~2.5, indicating the aggregates are quite compact, but not completely collapsed. This aggregation clearly impacts the dispersion and mobility of the covalent NOHMs particles in the solution, even at concentrations as low as 1 wt.%.

The fitting analysis of the covalent NOHMs solutions reveals that the SLD of the solvent is equal to that of D_2O (6.35E-06 $Å^{-2}$) and does not vary with NOHM concentration. In stark contrast to the ionic NOHM solutions, this indicates that there is *no free polymer* in the covalent NOHMs solution. The fitting analysis of the scattering also provides information on the grafted layer thickness of the covalent NOHMs particles in this solution, where Figure S7 plots the thickness of the grafted layer, showing that the length of the grafted NOHM-C-HPE polymer averages ~21Å.

It is well known that grafting density can significantly impact the grafted polymer height. At different grafting densities, the polymer can attain different conformations. At low grafting density, the polymer chains are relaxed in the mushroom region, which shifts to a semi-dilute polymer brush conformation at intermediate grafting densities.[54] Further packing of grafted polymer onto the surface forces an extended polymer brush conformation at high grafting density.[54] This study does not focus on the variation in polymer conformation with grafting density, but rather highlights the conformation of the polymer with the change in graft type. However, a study by McDonald et al. on similar covalent NOHMs suggests that the polymer chain with a grafting density of less than 0.8 chains nm^{-2} attains a mushroom conformation.[55] In this study, the maximum grafting density of covalent NOHMs is 0.7 chains nm^{-2} and, would suggest that our grafted polymer is in a relaxed state.

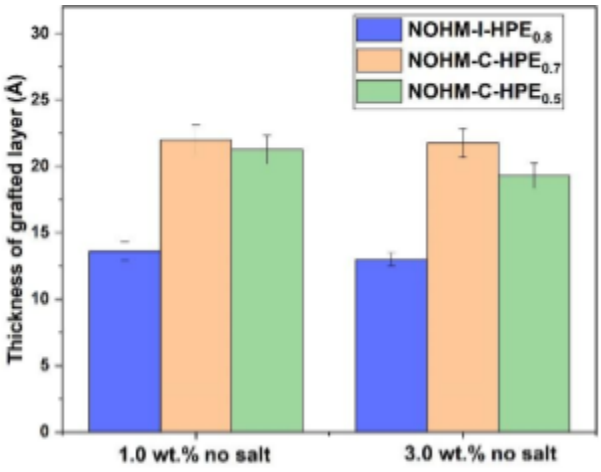

Figure 5. Thickness of grafted layer of NOHM-I-HPE$_{0.8}$, NOHM-C-HPE$_{0.7}$, NOHM-C-HPE$_{0.5}$ in aqueous solution.

Figure 5 clearly shows the role of the grafting type on the grafted layer thickness of the NOHM-I-HPE and NOHM-C-HPE. This data shows a stark contrast in the thickness of the grafted layers with the change in graft type. The thickness of the grafted layer of ionic NOHMs is significantly less than that of the covalent NOHMs, at similar grafting density. Even considering that some of the grafted polymer detaches in the ionic NOHMs, the maximum amount of free polymer present in the solvent is ~ 42 vol.%, which corresponds to a 'true' grafting density of ~0.5 chains nm^{-2} for the ionic NOHMs analyzed in this study. Our interpretation of this discrepancy is that the thickness of the

grafted polymer of ionic NOHMs obtained from the fitting parameter is not the actual thickness. Rather, the free polymer partially penetrates the grafted layer, which manifests as a reduction in the grafted layer thickness that emerges from the fitting, a phenomenon that is revealed in our previous SANS anlaysis.[47] Therefore, the thickness of the ionically grafted layer is not the actual thickness of the grafted polymer, rather it is the effective thickness of the grafted layer. While our previous finding of the interaction of free polymer with the grafted layer starts above 15 wt.%, the analyses performed in this study clearly show that the interaction of free polymer with the grafted layer is also present at low NOHMs loadings, as low as 1 wt.%, and in NOHMs systems that contain a much lower polymer grafting density. This variation in the assembly and structure of the grafted layer with the change in graft type, including the interaction of the free polymer with the grafted layer in the ionic NOHMs, will undoubtedly impact the performance and transport properties of these nanostructures in solution.

The fitting analysis also provides information on the amount of D_2O solvent penetrating the canopy/shell of the ionic and covalent NOHMs. Similar to Equation 1, Equation 2 shows the analytical relationship between the concentration of D_2O in the grafted layer (Φ_1) and the experimentally measured scattering length density (SLD) of the grafted layer in the NOHMs samples. In Equation 2, SLD of D_2O = 6.35E-06 Å^{-2}, SLD of polymer = 0.517E-06 Å^{-2} and SLD_{shell} is the experimentally determined SLD of the canopy that is obtained from fitting the scattering data of the ionic and covalent NOHMs solutions.

$$\Phi_1 = 1 - \frac{SLD_{D_2O} - SLD_{shell}}{SLD_{D_2O} - SLD_{poly}} \qquad \mathbf{2}$$

This analysis shows that the amount of D_2O penetrating the shell in the 1 wt.% ionic and covalent NOHMs are 90% and 60%, respectively. A high amount of D_2O penetration in the shell

of ionic NOHMs is consistent with an increase in free space near the nanoparticle surface due to the release of the grafted polymer from the corona. This results in more D_2O near the nanoparticle surface in ionic NOHMs than in covalent NOHMs.

Effect of salt addition on the structure and assembly of ionic and covalent NOHMs in solution:

The scattering curves of the NOHM-I-HPE and NOHM-C-HPE solutions with 0.1 M $KHCO_3$ were also measured and analyzed using the same scattering models for the solutions without salt. These analyses provide insight into the impact of adding salt to the NOHMs assembly and structure, including the grafted layer thickness of the NOHM-I-HPE and NOHM-C-HPE. Figure 6 plots the variation in the thickness of the grafted layer of the NOHM-I-HPE and NOHM-C-HPE in solution with a change in the amount of salt in the aqueous solution. Figure S8 shows the SANS profiles of NOHM-I-HPE and NOHM-C-HPE in the aqueous solution with salt.

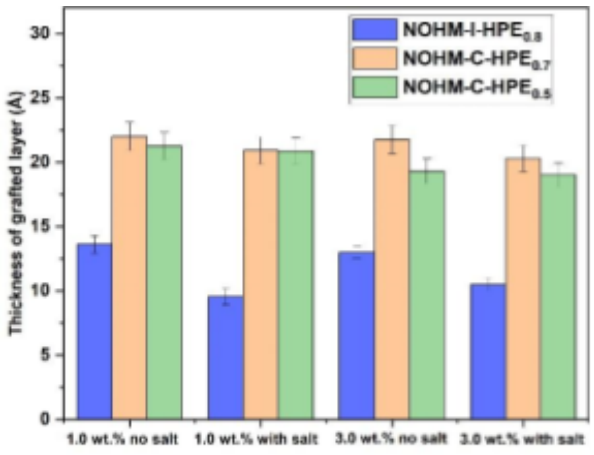

Figure 6. Thickness of grafted layer of $NOHM\text{-}I\text{-}HPE_{0.8}$, $NOHM\text{-}C\text{-}HPE_{0.7}$, $NOHM\text{-}C\text{-}HPE_{0.5}$ in aqueous solution with and without 0.1 M $KHCO_3$ salt.

With the addition of salt, the thickness of the grafted layer on NOHM-I-HPE decreases from ~14 Å to ~10 Å and the radius of gyration of the free polymer decreases from 13 Å to 12 Å. However, when salt is added to the NOHM-C-HPE solution, the assembly of NOHMs changes very slightly, where there is only a nominal change in grafted layer thickness. Thus, the addition

of salt significantly alters the structure of the grafted layer in ionic NOHMs, but not in the covalently bound NOHMs. This may be due to a change in the interaction of the free polymer with the grafted layer in the ionic NOHMs solutions. The addition of salt collapses the free polymer chain and subsequently decreases the interaction of the free polymer with the grafted layer. This allows grafted polymer to relax on the nanoparticle surface; thus, the grafted layer thickness decreases. Although our data indicates that the concentration of free polymer in the solution does not increase with the addition of salt, previous literature showed that the ions associated with the salt also compete with the HPE polymer to attach to the functionalized nanoparticle surface.[56,57] This is consistent with the D_2O penetration analysis of ionic NOHMs with the addition of salt, which is determined using Equation 2. With the addition of salt, the ionically grafted layer contains ~5% more D_2O than in the unsalted solution, while the covalently grafted layer only contains ~ 2.5% more D_2O than in the unsalted solution. This doubling of excess D_2O near the surface should correlate to more mobility within the grafted polymer layer, which may allow small ionic species to interact with functionalized nanoparticles.

Correlation of structural features of ionic and covalent NOHMs solutions with performance:

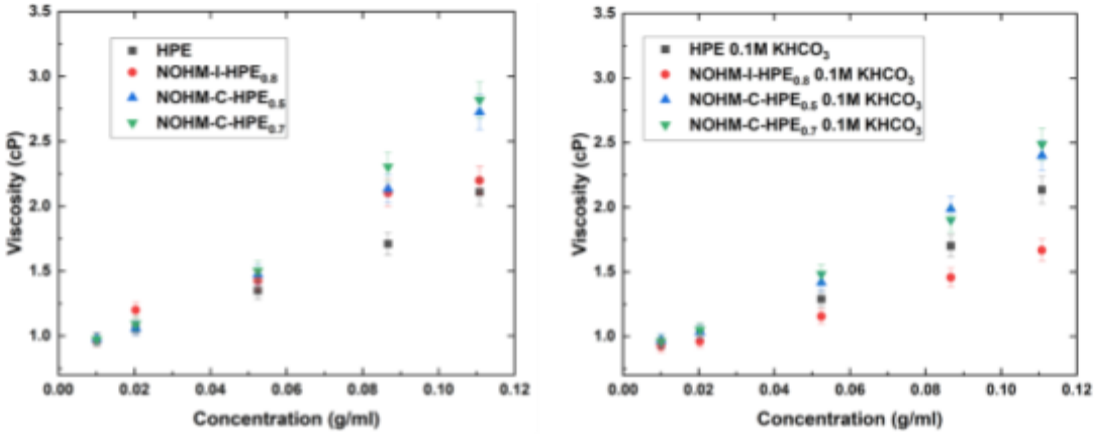

Figure SEQ Figure * ARABIC 7. Viscosity of HPE, NOHM-I-HPE$_{0.8}$, NOHM-C-HPE$_{0.7}$, NOHM-C-HPE$_{0.5}$ solutions with (right) and without 0.1 M $KHCO_3$ salt (left) as a function of solution concentration.

While the SANS results provide structural information of the NOHM-I-HPE and NOHM-C-HPE solutions, they do not offer direct insight into the transport properties that are relevant to their performance in electrochemical systems. To address this shortcoming, the structure of the NOHMs and HPE solutions are correlated to their viscosities. With this in mind, Figure 7 plots the viscosity of HPE polymer solutions, as well as those of the ionic and covalent NOHMs solutions with and without salt as a function of solute (NOHMs or HPE) concentration. These results, unsurprisingly, indicate that the viscosity of NOHMs solutions is higher relative to that of the HPE polymer in an aqueous solution. Previous studies have also found increasing viscosity with the presence of nanoparticles in the solution.[36,56,59] Moreover, the viscosities of the covalent NOHMs solutions are higher relative to that of the ionic NOHMs solutions. This can be correlated to the presence of the fractal aggregates in the covalent NOHMs solution, where the larger structure exhibits a larger viscosity.

It is interesting that as salt is added to the solution, the viscosity of the salted NOHM-I-HPE solution decreases drastically compared to that of the salted NOHM-C-HPE solution and the salted HPE solutions. This drastic decrease in the viscosity of ionic NOHMs may be correlated with the conformational results. The subtle decrease in the viscosity of NOHM-C-HPE correlates to the decrease in the grafted thickness of the polymer. The decrease in the viscosity of HPE polymer is also a result of decrease in size (radius of gyration) of the polymer chain. In the case of NOHM-I-HPE, the drastic decrease in viscosity may be due to the collapsed conformation of grafted layer on the silica nanoparticles, resulting in the decrease in the size of NOHMs particle.

To interrogate this possibility, the viscosity of the NOHM-I-HPE solution can be correlated to the size of the NOHM-I-HPE particle, including the grafted layer. The change in NOHM structure can be correlated to the change in the viscosity of the NOHM-I-HPE solutions using Einstein's viscosity equation documented as Equation 3.[60]

$$E = E_0 (1 + 2.5V) \qquad \mathbf{3}$$

Here, E is the viscosity of the solution, E_0 is the viscosity of the solvent, and V is the volume of the dispersed particles in the solution. By comparing the viscosities of the unsalted and salted NOHMs solutions for a given concentration, the relative change in size of the NOHM-I-HPE particles can be established. Using Equation 3 and the viscosities obtained for the NOHM-I-HPE solutions, this calculation shows that the volume of the NOHM-I-HPE in solution with no added salt is 1.9 times greater than the volume of the NOHM-I-HPE particle in solution in the presence of salt. This change in particle volume must be due to changes in the grafted layer, as the radius of the SiO_2 nanoparticle does not change. According to this analysis, the total grafted layer

thickness of the NOHM-I-HPE particle is *ca.* 23Å when no salt is present in the solution, while that of the NOHM-I-HPE particle is ~ 9.5 Å.

This is a little surprising in that the SANS analyses of the grafted layer of NOHM-I-HPE indicate that it is 13-15 Å, significantly less than 23 Å. We reconcile this apparent discrepancy by recalling that the SANS analyses represent the nominal grafted layer, i.e. the portion of the grafted layer that does not interact with the free polymer (See Figure 4). However, clearly, the size of the NOHM-I-HPE that impacts the viscosity is not just this nominal grafted layer. It makes more sense that the size of the SiO_2 nanoparticle, canopy, and free polymer that interacts with the canopy defines the size of the NOHM-I-HPE, which impacts the viscosity.

Figure 8 illustrates the structures of the NOHM-I-HPE that impact the flow behavior of the NOHMs solutions with and without salt, emphasizing the impact of the addition of salt on the grafted layer thickness of NOHM-I-HPE particles. The canopy of the NOHM that dictates the solution viscosity includes both the grafted polymer (light green) and interacting free polymer (dark green) to form a larger nanoparticle. The addition of salt collapses the grafted layer thickness, and the R_g of the free polymer, and the extent of interaction between the grafted layer and the grafted layer. The result in this case is that the canopy of the salted NOHM that impacts the

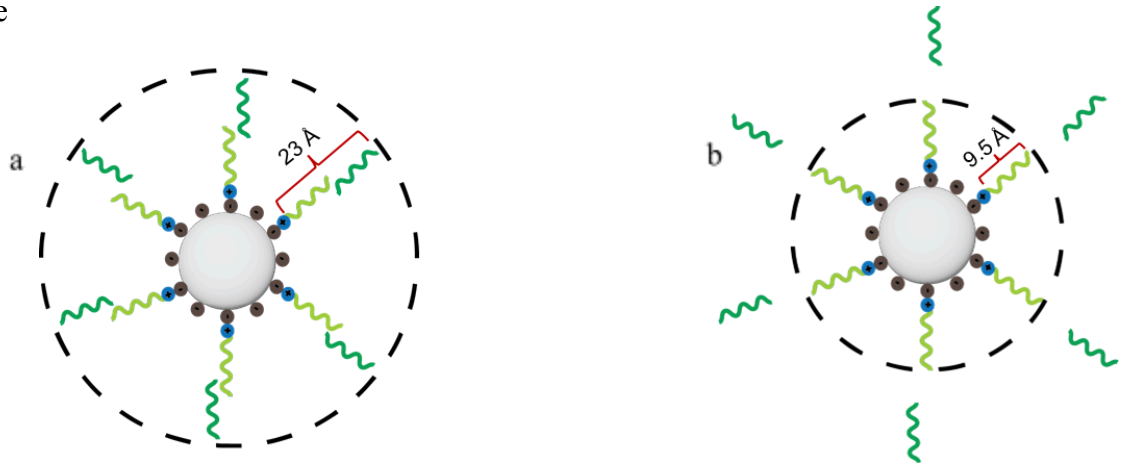

Figure 8. Illustration of the structure of NOHM-I-HPE with and without the presence of 0.1M KHCO... 8a. shows the canopy of the NOHM-I-HPE particle that includes both grafted polymer and

viscosity of the NOHM solution is dominated by the collapsed grafted layer, with little impact of the free polymer.

Thus, the careful analyses of the SANS data provide crucial insight into the role of the addition of salt on the conformation of the free polymer, on the size of the grafted layer, and correlates these structural characteristics to the viscosity of the salted ionic NOHMs solution. This insight provides important fundamental structure-property relationships that are needed to rationally design and implement NOHMs solutions in functional applications.

Conclusion

Small-angle neutron scattering experiments provide a critical understanding of the complex assembly and structure of NOHMs in aqueous solutions with a variation in bond type and added supporting electrolyte. Conformational analysis of untethered HPE polymer in aqueous solutions indicates that qualitatively, water is a θ (theta) solvent for the polymer and with added electrolyte, the quality of the solvent decreases, corresponding to a decrease in the size of the polymer. Our results highlight that the method of grafting the HPE polymer to the silica nanoparticles significantly alters the structure, assembly, and transport properties of NOHMs in solution. At a similar grafting density, the thickness of the grafted layer of ionic NOHMs is altered by the presence of free polymer. In contrast, the grafted layer of covalent NOHMs attains a corona thickness that is 1.5 times that of the grafted layer of ionic NOHMs. Moreover, the NOHM-C-HPE solution consists of aggregated particles alongside individually dispersed NOHM-C-HPE, which impacts the flow properties of the solutions, increasing the viscosity.

When salt is added to the NOHMs solutions, the assembly and structure of NOHM-I-HPE solution are altered more significantly than the NOHM-C-HPE solution. The addition of salt decreases the quality of the solvent, leading to a decrease in the size of the free polymer and collapse of the ionically grafted polymer layer on the nanoparticle surface. This results in reduced interaction between grafted and free polymer. These dramatic structural changes correlate to a significant reduction in viscosity. In the case of NOHM-C-HPE, a nominal change in the grafting layer thickness is observed with the addition of salt, corresponding to a slight change in the viscosity of the solutions. Thus, these results provide a holistic understanding of importance of grafting type on the structural features and dynamics of NOHMs in the presence of electro-active species that will contribute to improving the functionality of NOHMs in various applications.

Supporting Information

SANS profiles, graphical illustration of extent of aggregation in covalent NOHMs, thickness of grafted layer of covalent NOHMs.

Acknowledgment

Research supported as part of the Breakthrough Electrolytes for Energy Storage (BEES), an Energy Frontier Research Center funded by the U.S. Department of Energy (DOE), Office of Science, Basic Energy Sciences (BES), under Award DE-SC0019409 (neutron scattering experiments and analysis). A portion of this research was also completed at the High Flux Isotope Reactor a DOE Office of Science User Facility operated by the Oak Ridge National Laboratory. This work benefited from the use of the SasView application, originally developed under NSF award DMR-0520547. SasView contains code developed with funding from the

European Union's Horizon 2020 research and innovation program under the SINE2020 project, grant agreement No 654000.

Reference

(1) Dunn, B.; Kamath, H.; Tarascon, J. M. Electrical Energy Storage for the Grid: A Battery of Choices. *Science* **2011**, *334* (6058), 928–935. https://doi.org/10.1126/SCIENCE.1212741.

(2) Szetela, B.; Majewska, A.; Jamroz, P.; Djalilov, B.; Salahodjaev, R. Renewable Energy and CO_2 Emissions in Top Natural Resource Rents Depending Countries: The Role of Governance. *Front. Energy Res.* **2022**, *10*, 242. https://doi.org/10.3389/FENRG.2022.872941.

(3) Yang, Z.; Zhang, J.; Kintner-Meyer, M. C. W.; Lu, X.; Choi, D.; Lemmon, J. P.; Liu, J. Electrochemical Energy Storage for Green Grid. *Chem. Rev.* **2011**, *111* (5), 3577–3613. https://doi.org/10.1021/CR100290V.

(4) Chu, S.; Cui, Y.; Liu, N. The Path towards Sustainable Energy. *Nat. Mater.* **2016**, *16* (1), 16–22. https://doi.org/10.1038/NMAT4834.

(5) Soloveichik, G. L. Flow Batteries: Current Status and Trends. *Chem. Rev.* **2015**, *115* (20), 11533–11558. https://doi.org/10.1021/CR500720T.

(6) Chakrabarti, M. H.; Mjalli, F. S.; Alnashef, I. M.; Hashim, M. A.; Hussain, M. A.; Bahadori, L.; Low, C. T. J. Prospects of Applying Ionic Liquids and Deep Eutectic Solvents for Renewable Energy Storage by Means of Redox Flow Batteries. *Renew. Sustain. Energy Rev.* **2014**, *30*, 254–270. https://doi.org/10.1016/J.RSER.2013.10.004.

(7) Wei, X.; Hollas, A.; Yang, Z.; Huang, J.; Murugesan, V.; Walter, E.; Li, B.; Nie, Z.; Reed, D.; Zhang, Z.; Wang, W.; Sprenkle, V. Materials Development for Aqueous Organic Redox Flow Batteries. *ECS Meet. Abstr.* **2018**, *MA2018-01* (2), 239. https://doi.org/10.1149/MA2018-01/2/239.

(8) Winsberg, J.; Hagemann, T.; Janoschka, T.; Hager, M. D.; Schubert, U. S. Redox-Flow Batteries: From Metals to Organic Redox-Active Materials. *Angew. Chemie - Int. Ed.* **2017**, *56* (3), 686–711. https://doi.org/10.1002/anie.201604925.

(9) Nguyen, T.; Savinell, R. F. Flow Batteries. *Electrochem. Soc. Interface* **2010**, *19* (3), 54–56. https://doi.org/10.1149/2.F06103if.

(10) Lu, Y.; Chen, J. Prospects of Organic Electrode Materials for Practical Lithium Batteries. *Nat. Rev. Chem. 2020 43* **2020**, *4* (3), 127–142. https://doi.org/10.1038/s41570-020-0160-9.

(11) Huang, Z.; Kay, C. W. M.; Kuttich, B.; Rauber, D.; Kraus, T.; Li, H.; Kim, S.; Chen, R. An "Interaction-Mediating" Strategy towards Enhanced Solubility and Redox Properties of Organics for Aqueous Flow Batteries. *Nano Energy* **2020**, *69*, 104464.

https://doi.org/10.1016/J.NANOEN.2020.104464.

(12) Ejigu, A.; Greatorex-Davies, P. A.; Walsh, D. A. Room Temperature Ionic Liquid Electrolytes for Redox Flow Batteries. *Electrochem. commun.* **2015**, *54*, 55–59. https://doi.org/10.1016/J.ELECOM.2015.01.016.

(13) Imel, A. E.; Barth, B.; Hayes, D. G.; Dadmun, M.; Zawodzinski, T. Microemulsions as Emerging Electrolytes: The Correlation of Structure to Electrochemical Response. *ACS Appl. Mater. Interfaces* **2022**, *14* (17), 20179–20189. https://doi.org/10.1021/acsami.2c00181.

(14) Barth, B. A.; Imel, A.; Nelms, K. M. K.; Goenaga, G. A.; Zawodzinski, T. Microemulsions: Breakthrough Electrolytes for Redox Flow Batteries. *Front. Chem.* **2022**, *10*. https://doi.org/10.3389/FCHEM.2022.831200.

(15) Peng, J.; Xiao, Y.; Imel, A.; Barth, B. A.; Cantillo, N. M.; Nelms, K. M. K.; Zawodzinski, T. A. Electrolyte Effects on the Electrochemical Performance of Microemulsions. *Electrochim. Acta* **2021**, *393*, 139048. https://doi.org/10.1016/J.ELECTACTA.2021.139048.

(16) Peng, J.; Cantillo, N. M.; Nelms, K. M. K.; Roberts, L. S.; Goenaga, G.; Imel, A.; Barth, B. A.; Dadmun, M.; Heroux, L.; Hayes, D. G.; Zawodzinski, T. Electron Transfer in Microemulsion-Based Electrolytes. *ACS Appl. Mater. Interfaces* **2020**, *12* (36), 40213–40219. https://doi.org/10.1021/ACSAMI.0C07028.

(17) Wang, Y.; Niu, Z.; Zheng, Q.; Zhang, C.; Ye, J.; Dai, G.; Zhao, Y.; Zhang, X. Zn-Based Eutectic Mixture as Anolyte for Hybrid Redox Flow Batteries OPEN. https://doi.org/10.1038/s41598-018-24059-x.

(18) Xu, Q.; Qin, L. Y.; Ji, Y. N.; Leung, P. K.; Su, H. N.; Qiao, F.; Yang, W. W.; Shah, A. A.; Li, H. M. A Deep Eutectic Solvent (DES) Electrolyte-Based Vanadium-Iron Redox Flow Battery Enabling Higher Specific Capacity and Improved Thermal Stability. *Electrochim. Acta* **2019**, *293*, 426–431. https://doi.org/10.1016/J.ELECTACTA.2018.10.063.

(19) Kawase, K.; Abe, J.; Tenjimbayashi, M.; Kobayashi, Y.; Takahashi, K.; Shiratori, S. Novel Deep-Eutectic-Solvent-Infused Carbon Nanofiber Networks as High Power Density Green Battery Cathodes. *ACS Appl. Mater. Interfaces* **2018**, *10* (18), 15742–15750. https://doi.org/10.1021/ACSAMI.8B03099.

(20) Petit, C.; Bhatnagar, S.; Park, A. H. A. Effect of Water on the Physical Properties and Carbon Dioxide Capture Capacities of Liquid-like Nanoparticle Organic Hybrid Materials and Their Corresponding Polymers. *J. Colloid Interface Sci.* **2013**, *407*, 102–108. https://doi.org/10.1016/J.JCIS.2013.05.065.

(21) Feric, T. G.; Hamilton, S. T.; Haque, M. A.; Jeddi, J.; Sangoro, J.; Dadmun, M. D.; Park, A. H. A. Impacts of Bond Type and Grafting Density on the Thermal, Structural, and Transport Behaviors of Nanoparticle Organic Hybrid Materials-Based Electrolytes. *Adv. Funct. Mater.* **2022**, *32* (36). https://doi.org/10.1002/adfm.202203947.

(22) Feric, T. G.; Hamilton, S. T.; Park, A. H. A. Insights into the Enhanced Oxidative Thermal Stability of Nanoparticle Organic Hybrid Materials Developed for Carbon Capture and

Energy Storage. *Energy and Fuels* **2021**, *35* (23), 19592–19605. https://doi.org/10.1021/ACS.ENERGYFUELS.1C03243.

(23) Andrew Lin, K. Y.; Park, Y.; Petit, C.; Park, A. H. A. Thermal Stability, Swelling Behavior and CO2 Absorption Properties of Nanoscale Ionic Materials (NIMs). *RSC Adv.* **2014**, *4* (110), 65195–65204. https://doi.org/10.1039/c4ra10722e.

(24) Petit, C.; Lin, K. Y. A.; Park, A. H. A. Design and Characterization of Liquidlike POSS-Based Hybrid Nanomaterials Synthesized via Ionic Bonding and Their Interactions with CO_2. *Langmuir* **2013**, *29* (39), 12234–12242. https://doi.org/10.1021/LA4007923.

(25) Moon, S.; Lee, Y.; Choi, S.; Hong, S.; Lee, S.; Park, A.-H. A.; Park, Y. Spectroscopic Investigation of Thermochemical Depolymerization of Lignin Model Compounds in the Presence of Novel Liquidlike Nanoparticle Organic Hybrid Solvents for Efficient Biomass Valorization. **2018**. https://doi.org/10.1021/acs.oprd.8b00282.

(26) Lin, K.-Y. A. Y. A.; Park, A. H. A. Effects of Bonding Types and Functional Groups on CO_2 Capture Using Novel Multiphase Systems of Liquid-like Nanoparticle Organic Hybrid Materials. *Environ. Sci. Technol.* **2011**, *45* (15), 6633–6639. https://doi.org/10.1021/es200146g.

(27) Rim, G.; Feric, T. G.; Moore, T.; Park, A. H. A. Solvent Impregnated Polymers Loaded with Liquid-Like Nanoparticle Organic Hybrid Materials for Enhanced Kinetics of Direct Air Capture and Point Source CO_2 Capture. *Adv. Funct. Mater.* **2021**, *31* (21), 2010047. https://doi.org/10.1002/ADFM.202010047.

(28) Choudhury, S.; Agrawal, A.; Wei, S.; Jeng, E.; Archer, L. A. Hybrid Hairy Nanoparticle Electrolytes Stabilizing Lithium Metal Batteries. *Chem. Mater.* **2016**, *28* (7), 2147–2157. https://doi.org/10.1021/acs.chemmater.6b00029.

(29) Agrawal, A.; Choudhury, S.; Archer, L. A. A Highly Conductive, Non-Flammable Polymer–Nanoparticle Hybrid Electrolyte. *RSC Adv.* **2015**, *5* (27), 20800–20809. https://doi.org/10.1039/C5RA01031D.

(30) Tikekar, M. D.; Archer, L. A.; Koch, D. L. Stability Analysis of Electrodeposition across a Structured Electrolyte with Immobilized Anions. *J. Electrochem. Soc.* **2014**, *161* (6), A847–A855. https://doi.org/10.1149/2.085405JES.

(31) Park, Y.; Shin, D.; Jang, Y. N.; Park, A. H. A. CO_2 Capture Capacity and Swelling Measurements of Liquid-like Nanoparticle Organic Hybrid Materials via Attenuated Total Reflectance Fourier Transform Infrared Spectroscopy. *J. Chem. Eng. Data* **2011**, *57* (1), 40–45. https://doi.org/10.1021/JE200623B.

(32) Petit, C.; Park, Y.; Lin, K. Y. A.; Park, A. H. A. Spectroscopic Investigation of the Canopy Configurations in Nanoparticle Organic Hybrid Materials of Various Grafting Densities during CO_2 Capture. *J. Phys. Chem. C* **2012**, *116* (1), 516–525. https://doi.org/10.1021/JP210391C.

(33) Park, Y.; Petit, C.; Han, P.; Alissa Park, A.-H. H. Effect of Canopy Structures and Their Steric Interactions on CO_2 Sorption Behavior of Liquid-like Nanoparticle Organic Hybrid Materials. *RSC Adv.* **2014**, *4* (17), 8723–8726. https://doi.org/10.1039/c3ra46801a.

(34) Park, Y.; Decatur, J.; Lin, K. Y. A.; Park, A. H. A. Investigation of CO_2 Capture Mechanisms of Liquid-like Nanoparticle Organic Hybrid Materials via Structural Characterization. *Phys. Chem. Chem. Phys.* **2011**, *13* (40), 18115–18122. https://doi.org/10.1039/C1CP22631B.

(35) Feric, T. G.; Hamilton, S. T.; Ko, B. H.; Lee, G. A.; Verma, S.; Jiao, F.; Park, A. H. A. Highly Tunable Syngas Product Ratios Enabled by Novel Nanoscale Hybrid Electrolytes Designed for Combined CO_2 Capture and Electrochemical Conversion. *Adv. Funct. Mater.* **2023**, 2210017. https://doi.org/10.1002/ADFM.202210017.

(36) Lin, K.-Y. A.; Petit, C.; Park, A.-H. A. Effect of SO_2 on CO_2 Capture Using Liquid-like Nanoparticle Organic Hybrid Materials. *Energy & Fuels* **2013**, *27* (8), 4167–4174. https://doi.org/10.1021/ef400374q.

(37) Lin, K. Y. A.; Yang, H.; Lee, W. Der; Tsao, K. Y. A Magnetic Fluid Based on Covalent-Bonded Nanoparticle Organic Hybrid Materials (NOHMs) and Its Decolorization Application in Water. *J. Mol. Liq.* **2015**, *204*, 50–59. https://doi.org/10.1016/J.MOLLIQ.2015.01.020.

(38) Overa, S.; Feric, T. G.; Alissa Park, A.-H.; Jiao, F. Tandem and Hybrid Processes for Carbon Dioxide Utilization. **2021**. https://doi.org/10.1016/j.joule.2020.12.004.

(39) Feric, T. G.; Hamilton, S. T.; Cantillo, N. M.; Imel, A. E.; Zawodzinski, T. A.; Park, A. H. A. Dynamic Mixing Behaviors of Ionically Tethered Polymer Canopy of Nanoscale Hybrid Materials in Fluids of Varying Physical and Chemical Properties. *J. Phys. Chem. B* **2021**, *125* (32), 9223–9234. https://doi.org/10.1021/ACS.JPCB.1C00935.

(40) Hamilton, S. T.; Feric, T. G.; Bhattacharyya, S.; Cantillo, N. M.; Greenbaum, S. G.; Zawodzinski, T. A.; Park, A. A. Nanoscale Hybrid Electrolytes with Viscosity Controlled Using Ionic Stimulus for Electrochemical Energy Conversion and Storage. *JACS Au* **2022**. https://doi.org/10.1021/jacsau.1c00410.

(41) Zhang, Y.; Poe, D.; Heroux, L.; Squire, H.; Doherty, B. W.; Long, Z.; Dadmun, M.; Gurkan, B.; Tuckerman, M. E.; Maginn, E. J. Liquid Structure and Transport Properties of the Deep Eutectic Solvent Ethaline. *J. Phys. Chem. B* **2020**, *124* (25), 5251–5264. https://doi.org/10.1021/ACS.JPCB.0C04058.

(42) Klein, J. M.; Squire, H.; Dean, W.; Gurkan, B. E. From Salt in Solution to Solely Ions: Solvation of Methyl Viologen in Deep Eutectic Solvents and Ionic Liquids. **2020**. https://doi.org/10.1021/acs.jpcb.0c03296.

(43) Gurkan, B.; Squire, H.; Pentzer, E. Metal-Free Deep Eutectic Solvents: Preparation, Physical Properties, and Significance. *Journal of Physical Chemistry Letters*. 2019, pp 7956–7964. https://doi.org/10.1021/acs.jpclett.9b01980.

(44) Liu, S.; Tyagi, M.; Akcora, P. Polymer-Coupled Local Dynamics Enhances Conductivity of Ionic Liquids. *Macromolecules* **2020**, *53* (15), 6538–6546. https://doi.org/10.1021/ACS.MACROMOL.0C01434.

(45) Jayakody, N. K.; Fraenza, C. C.; Greenbaum, S. G.; Ashby, D.; Dunn, B. S. NMR Relaxometry and Diffusometry Analysis of Dynamics in Ionic Liquids and Ionogels for

Use in Lithium-Ion Batteries. *J. Phys. Chem. B* **2020**, *124* (31), 6843–6856. https://doi.org/10.1021/acs.jpcb.0c02755.

(46) Cantillo, N.; Bruce, M.; Hamilton, S.; Feric, T.; Park, A.-H. A.; Zawodzinski, T. Electrochemical Behavior of Copper Ion Complexed with Nanoparticle Organic Hybrid Materials. *J. Electrochem. Soc.* **2020**, *167* (11), 116508. https://doi.org/10.1149/1945-7111/aba158.

(47) Haque, M. A.; Feric, T.; Hamilton, S.; Park, A.-H.; Dadmun, M. Structure and Dispersion of Free and Grafted Polymer in Nanoparticle Organic Hybrid Materials-Based Solutions by Small-Angle Neutron Scattering. *J. Phys. Chem. C 125* (9), 5327–5334. https://doi.org/10.1021/acs.jpcc.0c10790.

(48) Choi, S.; Moon, S.; Park, Y. Spectroscopic Investigation of Entropic Canopy-Canopy Interactions of Nanoparticle Organic Hybrid Materials. *Langmuir* **2020**, *36* (32), 9626–9633. https://doi.org/10.1021/ACS.LANGMUIR.0C01784.

(49) SasView - Small Angle Scattering Analysis https://www.sasview.org/ (accessed Dec 8, 2021).

(50) Beaucage, G. Small-Angle Scattering from Polymeric Mass Fractals of Arbitrary Mass-Fractal Dimension. *J. Appl. Crystallogr.* **1996**, *29* (2), 134–146. https://doi.org/10.1107/S0021889895011605.

(51) Lodge, T. P.; Hiemenz, P. C. Polymer Chemistry. **2020**. https://doi.org/10.1201/9780429190810.

(52) Mildner, D. F. R.; Hall, P. L. Small-Angle Scattering from Porous Solids with Fractal Geometry. *J. Phys. D. Appl. Phys.* **1986**, *19* (8), 1535. https://doi.org/10.1088/0022-3727/19/8/021.

(53) Tomchuk, O. V.; Avdeev, M. V.; Bulavin, L. A. Modeling Fractal Aggregates of Polydisperse Particles with Tunable Dimension. *Colloids Surfaces A Physicochem. Eng. Asp.* **2020**, *605*, 125331. https://doi.org/10.1016/J.COLSURFA.2020.125331.

(54) Fernandes, N. J.; Koerner, H.; Giannelis, E. P.; Vaia, R. A. Hairy Nanoparticle Assemblies as One-Component Functional Polymer Nanocomposites: Opportunities and Challenges. *MRS Commun.* **2013**, *3* (1), 13–29. https://doi.org/10.1557/MRC.2013.9.

(55) Mcdonald, S.; Wood, J. A.; Fitzgerald, P. A.; Craig, V. S. J.; Warr, G. G.; Atkin, R. Interfacial and Bulk Nanostructure of Liquid Polymer Nanocomposites. **2015**. https://doi.org/10.1021/acs.langmuir.5b00255.

(56) Jespersen, M. L.; Mirau, P. A.; von Meerwall, E. D.; Koerner, H.; Vaia, R. A.; Fernandes, N. J.; Giannelis, E. P. Hierarchical Canopy Dynamics of Electrolyte-Doped Nanoscale Ionic Materials. **2013**, *46*, 31. https://doi.org/10.1021/ma402002a.

(57) Yu, Z.; Yang, F.; Dai, S.; Qiao, R. Structure and Dynamics of Polymeric Canopies in Nanoscale Ionic Materials: An Electrical Double Layer Perspective. *Sci. Reports 2018 81* **2018**, *8* (1), 1–11. https://doi.org/10.1038/s41598-018-23493-1.

(58) Mahbubul, I. M.; Saidur, R.; Amalina, M. A. Latest Developments on the Viscosity of

Nanofluids. *Int. J. Heat Mass Transf.* **2012**, *55* (4), 874–885. https://doi.org/10.1016/J.IJHEATMASSTRANSFER.2011.10.021.

(59) Olayiwola, S. O.; Dejam, M. Experimental Study on the Viscosity Behavior of Silica Nanofluids with Different Ions of Electrolytes. *Ind. Eng. Chem. Res.* **2020**, *59* (8), 3575–3583. https://doi.org/10.1021/ACS.IECR.9B06275.

(60) Mardles, E. W. J. Viscosity of Suspensions and the Einstein Equation [2]. *Nature*. Nature Publishing Group 1940, p 970. https://doi.org/10.1038/145970a0.

TOC Figure

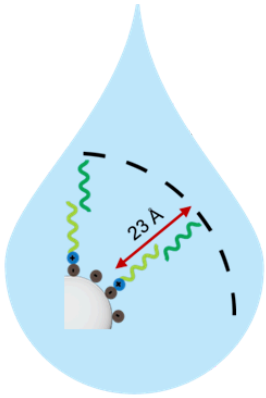

NOHM-I-HPE in aqueous solution

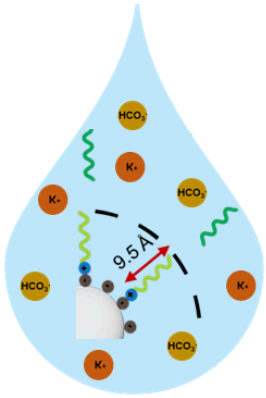

NOHM-I-HPE in aqueous solution with 0.1 M $KHCO_3$

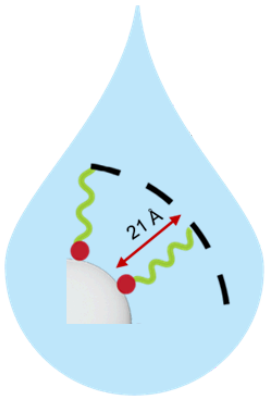

NOHM-C-HPE in aqueous solution

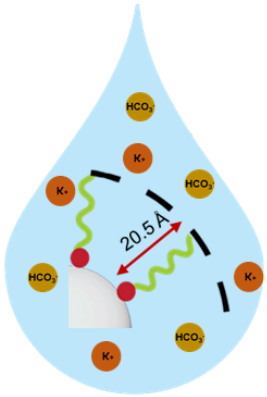

NOHM-C-HPE in aqueous solution with 0.1 M $KHCO_3$